Parametrization of the nuclear structure function

G. R. Boroun * and B. Rezaei †

Department of Physics, Razi University, Kermanshah 67149, Iran

(Received 8 November 2022; accepted 30 January 2023; published 27 February 2023)

In this paper, the parametrization of the nuclear structure function, which is directly constrained by the dynamics of QCD in its high-energy limit, is considered. This simple parametrization of the nuclear structure function is obtained from the proton experimental data by relying on a Froissart-bounded parametrization of the proton structure function. This phenomenological model describes high-energy QCD in the presence of saturation effects. Numerical calculations and comparison with available data from the NMC, EMC, and E665 Collaborations demonstrate that the suggested method by Armesto, Salgado, and Wiedemann (the ASW model) provides a reliable ratio of the nuclear structure functions F_2^A/AF_2^p at low x for light and heavy nuclei. The magnitude of nuclear shadowing is predicted for various kinematic regions and can be applied as well in the analysis of ultrahigh-energy processes by future experiments at electron-ion colliders.

DOI: 10.1103/PhysRevC.107.025209

I. INTRODUCTION

The knowledge of QCD dynamics at high energies is essential in the investigation of hadronic structure studied at current accelerators (JLab, RHIC, and the LHC) and future accelerators with the Electron-Ion Collider (EIC), Large Hadron electron Collider (LHeC), and Future Circular Collider (FCC) on the horizon. One of the main goals of high-energy nuclear physics is to comprehend the substructure of nucleons in the framework of QCD, which is a successful theory in describing the hadronic and nuclear phenomena as well as the inner structure of nucleons and nuclei. In this regard, the structure functions of nucleon and nuclei have played a crucial role. Nuclear structure functions measured in deep-inelastic scattering (DIS) experiments (which have been performed by NMC, SLAC, NMC, FNAL, BCDMS, HERMES, and JLAB groups) offer valuable information for understanding the dynamics of partons in the nuclear environment. The correct characterization of nuclear effects in the parton distribution functions (PDFs) is important due to their relevance in the determination of the proton PDFs and this is a baseline for new phenomena in heavy-ion collisions.

Nuclear parton distributions functions (nPDFs) are needed in the computation of inclusive cross sections of hard, factorizable, processes in high-energy nuclear collisions. The nuclear effects are generally added as a modification of baseline PDFs, either by expanding the parametrization or multiplying it by a factor, as reported in Refs. [1–12]. There is, in both cases, a dependence on the atomic mass number A. For this reason, there is a continual need for new data sets to broaden global analyses. In this way, groups like EPPS [13], NNPDF [14], or nCTEQ [15] have demonstrated the nucleon and nuclear PDF (nPDF) analyses in recent years. Nuclear effects on parton distributions and structure functions are important for interpreting high-energy processes involving nuclei such as heavy ions and electron-nucleus collisions at EIC [16] and LHeC/FCC [17]. These colliders (i.e., EIC and LHeC/FCC) are constructive in understanding the momentum distribution of quarks and gluons in nuclei.

At small values of the Bjorken variable x, the nonlinear QCD effects considered in these colliders are related to the studies of partonic structure of protons and nuclei [18,19]. The proposed LHeC collider covers a wide kinematical range down to $x \approx 10^{-6}$ in the perturbative range $Q^2 \gtrsim 1$ GeV^2, making it an ideal machine to study small-x physics. In addition to the Large Hadron-electron Collider, the construction of an Electron-Ion Collider with a possibility to operate with a wide variety of nuclei will allow one to explore the low-x region in much greater detail. In this region a transition between linear and nonlinear scale evolution of the parton densities will be crucial [20]. The latter regime, known as "saturation" [21,22], occurs at low x and low interaction scale Q^2 where the recombination of low-x gluons becomes increasingly important.

Also, the small-x region of QCD can be described theoretically in the effective-field theory known as the Color Glass Condensate (CGC); see Ref. [23] for a review. In the CGC picture the nonlinear evolution equations describe the evolution of the small-x gluon fields. Probing these nonlinearities at the LHeC and EIC are crucial to test the saturation picture [18]. These nonlinearities are important in electron-nucleus scattering in comparison with electron-proton interactions. The

*boroun@razi.ac.ir
†brezaei@razi.ac.ir

Published by the American Physical Society under the terms of the Creative Commons Attribution 4.0 International license. Further distribution of this work must maintain attribution to the author(s) and the published article's title, journal citation, and DOI. Funded by SCOAP^3.

Hadron Electron Ring Accelerator (HERA) did not report the nonlinear behavior of the distribution functions in deep-inelastic scattering off nuclei at collider energies. Despite this, future colliders (such as LHeC and EIC) will offer unique capabilities to answer the nonlinearity in nuclei at high energies [20,24].

The proposed EIC would enable the first direct measurements of nuclear gluons at intermediate and large x by using heavy quark probes and could qualitatively advance our understanding of the gluonic structure of nuclei [25]. This collider (i.e., EIC) would have a strong impact, in particular on understanding the small- and large-x regions of nuclear shadowing and the EMC effect in comparison with fixed-target kinematics, which DIS data considerably restricts in range in x and Q^2, and only with limited statistics for various nuclei [26]. The experiment at EIC is DIS off a proton or a nucleus with the variable center-of-mass energy within the range $20 < \sqrt{s} < 140$ GeV, where this is lower than at HERA with $\sqrt{s} = 318$ GeV, but the luminosity is higher by a factor of 1000. The EIC will combine the experience from HERA to deliver polarized electron beams with the experience from RHIC to be the first machine that provides the collision of polarized electrons with polarized protons, and at a later stage, polarized ^{2}H and ^{3}He [27]. At fixed-target facilities, such as JLab, the majority of the momentum is carried by the electron, while for electron-ion collider experiments, the majority of the momentum is carried by the ion beam, so variables are defined according to the electron beam and the ion beam (against the electron beam), respectively. A detailed description of the fixed-target and the EIC four-momenta is given in Ref. [28]. For collider experiments, the center-of-mass energy $\sqrt{s_{\rm EIC}} = \sqrt{4E_eE_h}$ is often used as a frame of reference and for fixed-target experiments the center-of-mass energy $\sqrt{s_{\rm JLab}} = (2m_hE_e + m_h^2)^{1/2}$, where $E_h = m_h$ (target mass). The familiar definitions of the Bjorken x are significantly different between EIC and fixed-target experiments: for fixed-target experiments $x_{\rm Fixed} = Q^2/(2m_h\nu)$ where ν is the energy transform $\nu = E_e - E'_e$. At JLab, the Bjorken-x scaling is defined as $x_{\rm JLab} = Nx_{\rm Fixed}$, where N is the number of nucleons in the target. In collider experiments, $x = x_p/N$ where $x_p = Q^2/[2E_p(\nu + \nu_z)]$ and $\nu_z = E_e - E'_e \cos\theta_e$. Also, the collider definition of W^2 is $W^2 = Q^2(1-x)/x$ where, in fixed-target experiments, it is modified by $W^2_{\rm JLab} = m_p^2 + Q^2(1-x_{\rm JLab})/x_{\rm JLab}$. Therefore, the kinematic (x, Q^2) range of the fixed-target experiments will be tested by EIC, as discussed in Ref. [28].

The simplest observable to study nuclear effects is to measure the structure function ratios at small x ($x \leqslant 0.01$, shadowing region). Indeed, the structure function F_2 per nucleon turns out to be smaller in nuclei than in a free nucleon [24] and this is very important for the study of nuclear structure and nuclear collisions. Nuclear shadowing is a consequence of multiple scattering because this is well understood in the gluon recombination. Indeed, in the frame in which the nucleus is moving fast, the gluon clouds from different nucleons overlap. Therefore the ratio of the structure functions (i.e., F_2^A/AF_2^p), at small x, is smaller than 1. The shadowing effect is well understood by the characteristic momentum scale which is known as the saturation scale Q_s^2. This scale (i.e., saturation scale) increases with decreasing x as $Q_s^2 = Q_0^2(x/x_0)^{-\lambda}$. Geometrical scaling for $\alpha_s(Q^2)xg(x, Q^2)/Q^2$ holds at the boundary $Q^2 = Q_s^2$. For $Q^2 < Q_s^2$ the linear evolution is strongly perturbed by nonlinear effects and for $Q^2 > Q_s^2$ the nonlinear screening effects can be neglected [29].

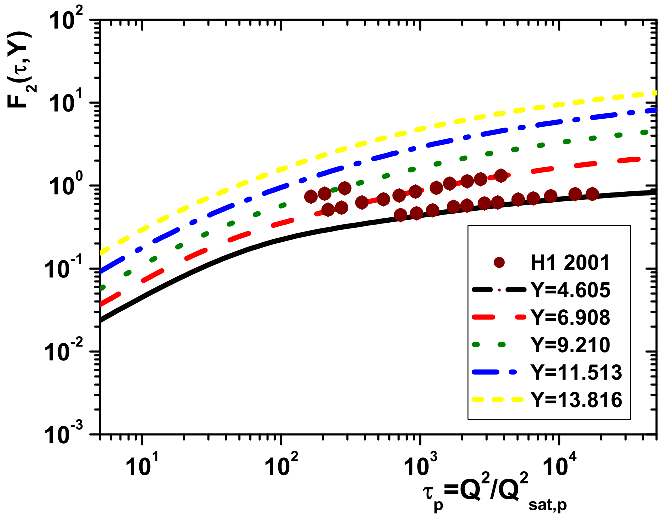

FIG. 1. The proton structure function $F_2(\tau, Y)$ plotted versus scaling variable $\tau_p = Q^2/Q^2_{\rm sat,p}$ for different values of rapidities $Y = \ln\frac{1}{x}$ from $Y_{\rm min} = 4.605$ (solid curve) to $Y_{\rm max} = 13.816$ (short-dash curve) compared with the H1 Collaboration data as accompanied with total errors [40], for $x = 10^{-6}, \ldots, 10^{-2}$ (curves from up to down, respectively).

In this paper a simple parametrization for the nuclear structure function based on the parametrization of the proton structure function is proposed. In Ref. [30] authors have suggested parametrization of the proton structure function which describes fairly well the available experimental data on the reduced cross sections at small x where it is also pertinent in investigations of lepton-hadron processes at ultrahigh energies (i.e., the scattering of cosmic neutrinos from hadrons). The parametrization of the proton structure function describes all data on DIS in the region of $x \leqslant 0.01$ in a wide interval of photon virtualities [30]. Relying on saturation scaling arguments, a simple model for the parametrization of the nuclear structure function is suggested.

II. A MODEL FOR THE NUCLEAR STRUCTURE FUNCTION

It is customary to write the proton structure function F_2 into the cross sections $\sigma_{T,L}$ for the collision of the transversal (T) or longitudinal (L) virtual photon of momentum q, $q^2 = -Q^2$, on the proton as follows:

$$F_2^p(x, Q^2) = \frac{Q^2}{4\pi^2\alpha_{em}}[\sigma_T^{\gamma^*p}(x, Q^2) + \sigma_L^{\gamma^*p}(x, Q^2)]. \quad (1)$$

The electron-proton (ep) deep-inelastic scattering (DIS) data at small values of the Bjorken variable x can be described within the framework of the dipole model [24,31–35]. In the dipole frame, the incoming photon splits into a $q\bar{q}$, which then interacts with the proton. This process depends on the total

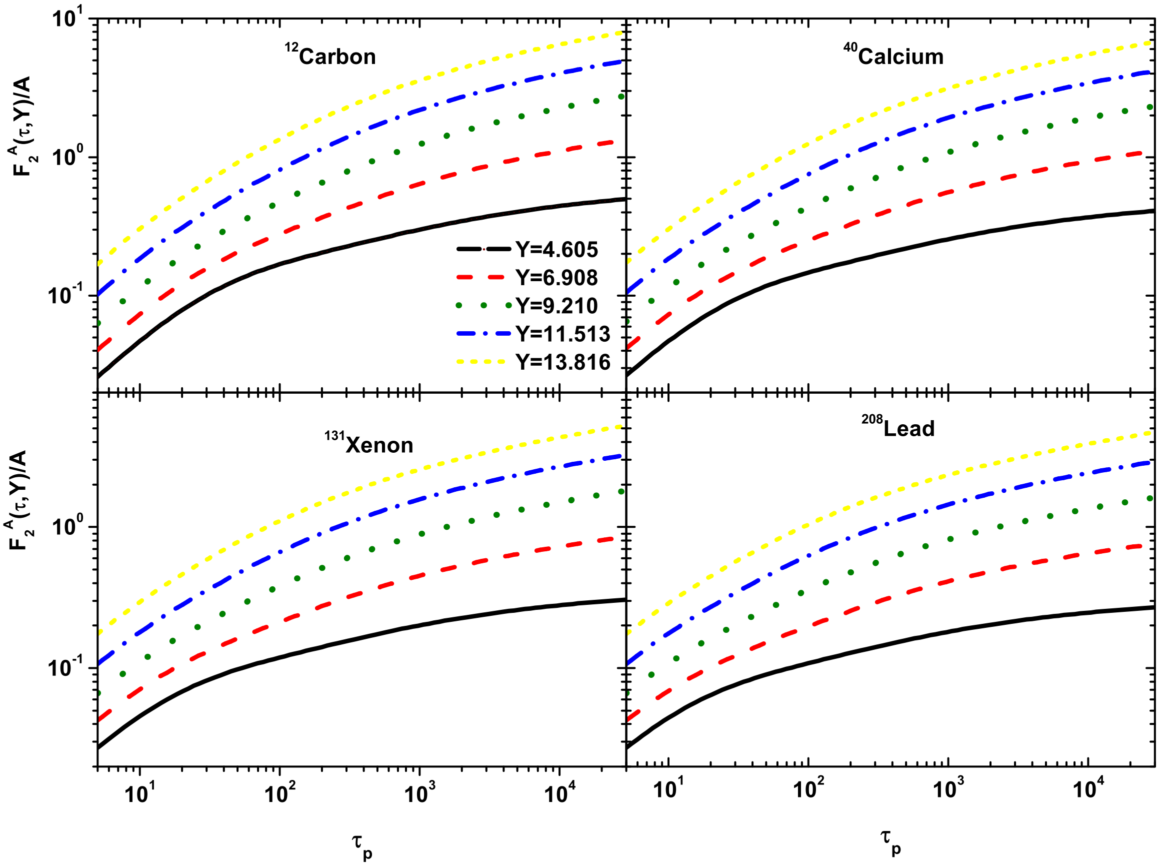

FIG. 2. The nuclear structure function $F_2^A(\tau, Y)$ (normalized to the number of nucleons) plotted versus scaling variable $\tau_p = Q^2/Q^2_{\text{sat,p}}$ for different values of rapidities $Y = \ln\frac{1}{x}$, from $Y_{\min} = 4.605$ (solid curve) to $Y_{\max} = 13.816$ (short-dash curve) for carbon, calcium, xenon and lead nuclei, for $x = 10^{-6}, \ldots, 10^{-2}$ (curves from up to down, respectively).

dipole-proton cross section, which varies with x and the transverse size r of the dipole. The total $\gamma^* p$ cross section reads

$$\sigma_{L,T}^{\gamma^* p}(Q^2, Y) = \int d^2\mathbf{r} \int_0^1 dz |\Psi_{L,T}(\mathbf{r}, z; Q^2)|^2 \sigma_{\text{dip}}^{\gamma^* p}(r, Y), \tag{2}$$

with $Y = \log(1/x)$ called the rapidity. $\Psi_{L,T}$ is the wave function for the splitting of the virtual photon into a $q\bar{q}$ pair (dipole) and $\sigma_{\text{dip}}^{\gamma^* p}(r, Y) = 2\pi R_p^2 N(r, Y)$ is the dipole-proton cross section where N is the dipole-proton scattering amplitude as entering the QCD evolution equations. Here z is a fraction of longitudinal photon momentum carried by quark and R_p is the radius of the proton. The wave function of the virtual photon, $|\Psi|^2 = |\Psi_T|^2 + |\Psi_L|^2$, in the leading order is given by

$$\begin{aligned} |\Psi_T(r, z; Q^2)|^2 &= \frac{3\alpha_{em}}{2\pi^2} \sum_f e_f^2 \{[z^2 + (1-z)^2]\overline{Q}_f^2 K_1^2(r\overline{Q}_f) \\ &\quad + m_f^2 K_0^2(r\overline{Q}_f)\}, \\ |\Psi_L(r, z; Q^2)|^2 &= \frac{3\alpha_{em}}{2\pi^2} \sum_f e_f^2 4Q^2 z^2 (1-z)^2 K_1^0(r\overline{Q}_f), \end{aligned} \tag{3}$$

where K_0 and K_1 are the Bessel functions, sums $\sum_f$ run over all quark flavors with charge e_f and mass m_f, and $\overline{Q}_f^2 = z(1-z)Q^2 + m_f^2$.

In the color-dipole formalism, the nuclear structure function (i.e., F_2^A) is proportional to the dipole nucleus cross section (i.e., $\sigma_{\text{dip}}^{\gamma^* A}$). $\sigma_{\text{dip}}^{\gamma^* A}$ describes the interaction of the $q\bar{q}$ dipole with the nucleus target. In the eikonal approximation, the total cross section for a dipole to scatter off the target nucleus at an impact parameter $\mathbf{b}$ is given by [1–4,19–35]

$$\sigma_{\text{dip}}^{\gamma^* A}(r, Y) = 2 \int d^2\mathbf{b} N_A(\mathbf{r}, Y; \mathbf{b}). \tag{4}$$

The nuclear scattering amplitude $N_A(\mathbf{r}, Y; \mathbf{b})$ depends on the impact parameter $\mathbf{b}$, rapidity, and dipole size $\mathbf{r}$.

The one dimensionless variable $\tau = Q^2/Q_s^2$ is the geometric scaling where the physics remains unchanged when one moves parallel to the saturation line. Indeed the saturation scale is a border between dense and dilute gluonic systems and the geometric scaling can be understood as a property of the small-x evolution equations in the large-rapidity regime. In Ref. [36], an analytic interpolation of lepton-proton data as function of the scaling variable $\tau = Q^2/Q_s^2$ was proposed. The ASW form of the single universal curve on $\sigma^{\gamma^* p}$ is given

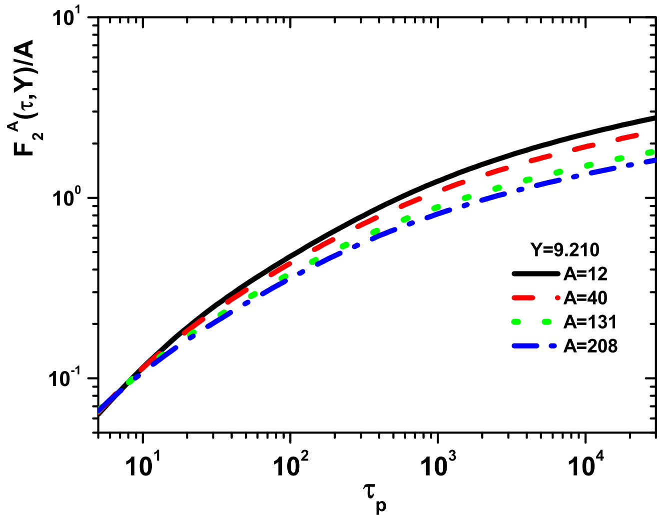

FIG. 3. A dependence of nuclear structure function (normalized to the number of nucleons) for $A = 12$, 40, 131, and 208 at $Y = 9.210$ ($x = 10^{-4}$) plotted versus scaling variable τ_p .

by [35]

$$\sigma^{\gamma^* p}(x, Q^2) \equiv \Phi(\tau) = \overline{\sigma}_0[\gamma_E + \Gamma(0, \xi) + \ln \xi], \tag{5}$$

where γ_E and $\Gamma(0, \xi)$ are the Euler constant and the incomplete Γ function, respectively. The authors of Ref. [35] extracted the ξ function from a fit to lepton-proton data as $\xi = a/\tau^b$ with $a = 1.868$ and $b = 0.746$. The normalization is fixed by $\overline{\sigma}_0 = 40.56$ μb and the saturation scale Q_s^2 is parametrized as $Q_s^2 = (1\ \text{GeV}^2)(\overline{x}/x_0)^{-\lambda}$, where $x_0 = 3.04\times10^{-4}$, $\lambda = 0.288$ and $\overline{x} = x(Q^2 + 4m_f^2)/Q^2$ with $m_f = 0.14$ GeV. The nuclear structure function is defined by $F_2^A(x, Q^2) = Q^2\sigma^{\gamma^* A}/(4\pi^2\alpha)$ where $\sigma^{\gamma^* A} = \frac{\pi R_A^2}{\pi R_p^2}\sigma^{\gamma^* p}(\tau_A)$ and R_A is the nuclear radius.

In Ref. [33], the authors have introduced the saturation scale $Q_s^2(Y) \propto \exp(\upsilon_c Y)$, where it is based on an analytic interpolation asymptotic behavior of the amplitude for the unintegrated gluon function. The dipole-proton (nucleus) scattering amplitude is as a result of the Balitsky-Kovchegov (BK) evolution equation [37,38] at high-energy evolution. $Q_s^2(Y)$ is obtained from the knowledge of the Balitsky-Fadin-Kuraev-Lipatov (BFKL) kernel [39] in the form [33]

$$Q_s^2(Y) = k_0^2 \exp(\overline{\alpha}\upsilon_c Y), \tag{6}$$

where the parameters of model have been determined according to the HERA data [40] as $\upsilon_c = 0.807$, $k_0^2 = 3.917\times10^{-3}$ GeV^2 and $\overline{\alpha} = 3\alpha_s/\pi$. The condition for geometric scaling in the case of $\gamma^* - A$ interactions is defined by the following form [33,35]:

$$\sigma_{\text{tot}}^{\gamma^* A}\left(\frac{Q^2}{Q_{s,A}^2}\right) = \left(\frac{\pi R_A^2}{\pi R_p^2}\right)\sigma_{\text{tot}}^{\gamma^* p}\left(\frac{Q^2}{Q_{s,A}^2}\right), \tag{7}$$

where

$$Q_{s,A}^2(Y) = Q_{s,p}^2(Y)\left(\frac{A\pi R_p^2}{\pi R_A^2}\right)^{1/\delta}, \tag{8}$$

and $Q_{s,p}(Y)$ [$\equiv Q_s(Y)$] is the saturation scale for a proton target. In the dipole model, the nuclear data are reproduced for $\delta = 0.79 \pm 0.02$ and $\pi R_p^2 = 1.55 \pm 0.02$ fm^2 at low values of x where the nuclear radius is given by the usual parametrization $R_A = (1.12A^{1/3} - 0.86A^{-1/3})$ fm [33,35,41,42]. In the region of small x, the effect of nuclear shadowing manifests itself as an inequality F_2^A/AF_2^p, where $\sigma^{\gamma^* A}/A\sigma^{\gamma^* p} \approx F_2^A/AF_2^p$. This leads to the following result for the nuclear structure function:

$$F_2^A(\tau_A, Y) = \left(\frac{\pi R_A^2}{\pi R_p^2}\right)F_2^p(\tau_A, Y), \tag{9}$$

where the geometric scaling is considered by the following form

$$\tau_A = \tau_p\left(\frac{\pi R_A^2}{A\pi R_p^2}\right)^{1/\delta}, \tag{10}$$

and $\tau_p \equiv \tau = Q^2/Q_s^2(Y)$. The explicit expression for the parametrization of the nuclear structure function F_2^A, is the same of the parametrization of the proton structure function with the change $Q^2 \to Q_A^2$, where

$$Q_A^2 = \tau\left(\frac{A\pi R_p^2}{\pi R_A^2}\right)^{1/\delta} Q_s^2 = \tau Q_{s,A}^2. \tag{11}$$

In Ref. [30] an analytical expression for the proton structure function, which describes fairly well the available experimental data on the reduced cross section in full accordance with the Froissart predictions, is defined by the following form:

$$F_2(x, Q^2) = D(Q^2)(1 - x)^n \sum_{m=0}^{2} A_m(Q^2)L^m. \tag{12}$$

Therefore the parametrization of the nuclear structure function [according to Eqs. (9)–(12)] reads

$$F_2^A(\tau, Y) = \left(\frac{\pi R_A^2}{\pi R_p^2}\right)D\big(\tau Q_{s,A}^2\big)(1 - e^{-Y})^n \times \sum_{m=0}^{2} A_m\big(\tau Q_{s,A}^2\big)L^m\big(\tau Q_{s,A}^2, Y\big), \tag{13}$$

where

$$D\big(Q_j^2\big) = \frac{Q_j^2\big(Q_j^2 + \lambda M^2\big)}{\big(Q_j^2 + M^2\big)^2}, \quad A_0\big(Q_j^2\big) = a_{00} + a_{01}L_2\big(Q_j^2\big),$$
$$A_i\big(Q_j^2\big) = \sum_{k=0}^{2} a_{ik}L_2\big(Q_j^2\big)^k, \quad i = (1, 2),$$
$$L\big(Q_j^2, Y\big) = Y + \ln\frac{Q_j^2}{Q_j^2 + \mu^2}, \quad L_2\big(Q_j^2\big) = \ln\frac{Q_j^2 + \mu^2}{\mu^2},$$
$$j = p, A. \tag{14}$$

The effective parameters are defined in Table I.

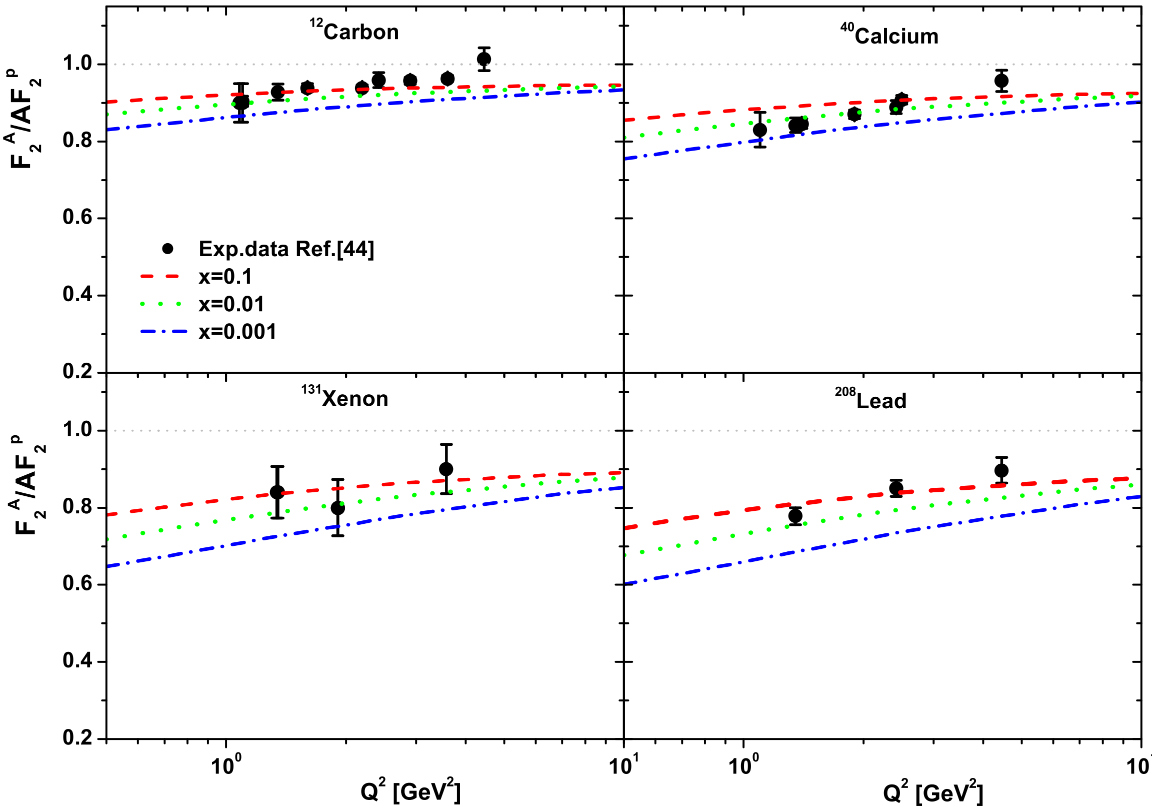

FIG. 4. The nuclear ratio F_2^A/AF_2^p with respect to the ASW model, as a function of Q^2 for several nuclear targets for $x = 10^{-1}, \ldots, 10^{-3}$ (curves from up to down, respectively), compared with the experimental data [44] (i.e., E665, EMC, and NMC Collaborations) as accompanied with total errors.

In the ASW model [35], the nucleon structure function is defined by the following form:

$$F_2^p(\tau) = \frac{Q_{s,p}^2 \tau_p}{4\pi^2\alpha}[\gamma_E + \Gamma(0, \xi_p) + \ln\xi_p]. \tag{15}$$

The explicit expression for the ratio in this model reads

$$\frac{F_2^A(\tau_A)}{AF_2^p(\tau)} = \left(\frac{\pi R_A^2}{\pi R_p^2}\frac{Q_{s,A}^2 \tau_A}{AQ_{s,p}^2 \tau_p}\right)\frac{\gamma_E + \Gamma(0, \xi_A) + \ln\xi_A}{\gamma_E + \Gamma(0, \xi) + \ln\xi}, \tag{16}$$

where $\xi_A = a/\tau_A^b$. Notice that Eq. (15) is written in the geometrical scaling whereas the Eq. (12) is in (x-Q^2) space.

TABLE I. The effective parameters at low x are defined by the Block-Halzen fit to the HERA data as $M^2 = 0.753 \pm 0.068$ GeV^2, $\mu^2 = 2.82 \pm 0.290$ GeV^2, $n = 11.49 \pm 0.99$, and $\lambda = 2.430 \pm 0.153$ [30].

Parameter	Value
a_{10}	$8.205\times10^{-4} \pm 4.62\times10^{-4}$
a_{11}	$-5.148\times10^{-2} \pm 8.19\times10^{-3}$
a_{12}	$-4.725\times10^{-3} \pm 1.01\times10^{-3}$
a_{20}	$2.217\times10^{-3} \pm 1.42\times10^{-4}$
a_{21}	$1.244\times10^{-2} \pm 8.56\times10^{-4}$
a_{22}	$5.958\times10^{-4} \pm 2.32\times10^{-4}$
a_{00}	$2.550\times10^{-1} \pm 1.600\times10^{-2}$
a_{01}	$1.475\times10^{-1} \pm 3.025\times10^{-2}$

Since the cross section in Eq. (7) only depends on Q^2/Q_s^2, the replacement $Q_{s,p}^2 \to Q_{s,A}^2$ corresponds to the rescaling $Q^2 \to Q^2/\lambda_A^2$ in Eq. (12), where $\lambda_A = (\frac{\pi R_A^2}{A\pi R_p^2})^{1/2\delta}$ [43].

III. RESULTS AND CONCLUSIONS

In this section, the numerical calculation of the nuclear structure function and the nuclear ratio using Eqs. (13) and (16) is investigated. With respect to these equations the nucleon and nuclear structure functions and the corresponding ratios for values $x \leqslant 0.01$ can be computed. Calculations have been performed at a fixed value of the running coupling. For the LO BFKL kernel, one finds $\upsilon_c = 0.807$ and $\upsilon_c = 4.88\overline{\alpha}$ [33], therefore, the coupling constant is fixed by $\alpha_s = 0.17$. The overlap between the models indicates that the Bjorken variable x varies in the interval $10^{-2} \leqslant x \leqslant 10^{-6}$ and Q^2 varies in the interval 0.15 GeV$^2 \leqslant Q^2 \leqslant 150$ GeV^2. In Fig. 1 the proton structure functions are presented as a function of scaling variable τ for different values of rapidities and compared with the H1 Collaboration data [40]. The proton structure functions obtained into the scaling variable τ are comparable with data of the H1 Collaboration. At intermediate and high scaling variable τ, the extracted proton structure functions are in a good agreement with experimental data. The parametrization of the proton structure function is translated to the nuclear structure function as quantified by Eq. (13). To investigate the parametrization model for the nuclear structure function we consider results obtained using the scaling variable τ for light and heavy nuclei. In Fig. 2 we show the nuclear structure function as a function of scaling variable τ for different values of rapidities and different nuclei. These theoretical curves are the result of the parametrization of the nuclear structure function, meaning that we are using the geometrical scaling in the parametrization method. Furthermore, we check the A dependence of the nuclear structure function at $Y = 9.210$ in Fig. 3. In Fig. 3, the nuclear structure function decreases as the atomic mass number A increases. It is clear that the A dependence of the nuclear structure function in electron-nucleus collisions at midrapidity involve additional nuclear effects which are at least as significant as nuclear shadowing. The parametrization method reported by authors in Ref. [35] can be covered all data on photon-nucleon and photon-nuclei, so we compared the nuclear ratio F_2^A/AF_2^p with the experimental data [44] in Fig. 4. Figure 4 compares our calculations of the shadowing due to the ASW model [Eq. (16)] with available data from the E665, EMC and EMC Collaborations [44]. The shadowing in nuclei is studied in this figure (i.e., Fig. 4) through the ratios of cross sections per nucleon for different nuclei at the Bjorken scaling values $x = 10^{-1}, \ldots, 10^{-3}$ respectively. We have selected data where $x < 0.03$ and accompanied with total errors. We observe that, for fixed x and large Q^2, the ratio become closer to one, i.e., shadowing decreases with increasing Q^2 and also a larger nuclear shadowing is visible for lead target at low Q^2. These results are comparable with others in Refs. [9,42]. In Refs. [9] and [42], nuclear shadowing in the Regge limit within the Glauber-Gribov model and in the color dipole formalism based on the rigorous Green's function techniques at small x have been considered, respectively. The behavior and magnitudes of shadowing using the both color dipole formalism from the higher $|q\bar{q}\rangle$ Fock component in Ref. [42] and the parametrization method are comparable. The predictions for expected scaling kinematics in experiments at EICs are presented in Fig. 4 for the C, Ca, Xe, and Pb targets. Also, the ASW model is in good agreement with the dipole model calculation of Ref. [45], where rescatterings of the full $q\bar{q} + Ng$ fluctuation is taken into account where the higher Fock states of the dipole correspond to the summation of triple-pomeron diagrams in that approach. Therefore, these predictions within the parametrization of the nuclear ratios, due to the ASW model, are comparable with other dipole models (such as GBW [46,47], KST [48], BGBK [49], IP-sat [50]).

In conclusion, we studied the shadowing in deep-inelastic scattering off nuclei in the kinematic regions accessible by the future electron-ion colliders with respect to the parametrization method and the ASW model, respectively. We presented a further development of the parametrization of the DIS structure function with respect to the saturation scaling. We calculated the shadowing of the nuclear structure function in the ASW model in the region of $x \leqslant 0.1$ in a wide interval of photon virtualities. Then we compared the magnitudes of shadowing using the ASW model for the light and heavy nuclei and showed that these predictions are in a good agreement with available data from the E665, EMC, and NMC Collaborations.

ACKNOWLEDGMENT

The authors are thankful to the Razi University for financial support of this project. Also, G.R.B. wishes to especially thank N. Armesto for reading and commenting on the paper.

[1] B. Nachman, K. Wichmann, and P. Zurita, SciPost Phys. Proc. **8**, 004 (2022).
[2] N. Armesto, H. Paukkunen, C. A. Salgado, and K. Tywoniuk, Phys. Lett. B **694**, 38 (2010).
[3] K. J. Eskola, H. Honkanen, V. J. Kolhinen, and C. A. Salgado, Phys. Lett. B **532**, 222 (2002).
[4] K. J. Eskola, H. Paukkunen, and C. A. Salgado, J. High Energy Phys. 07 (2008) 102; 04 (2009) 065.
[5] S. Kumano and M. Miyama, Phys. Lett. B **378**, 267 (1996); M. Arneodo, Phys. Rep. **240**, 301 (1994); D. F. Geesaman, K. Saito, and A. W. Thomas, Annu. Rev. Nucl. Part. Sci. **45**, 337 (1995).
[6] E. P. Segarra *et al.*, Phys. Rev. D **103**, 114015 (2021).
[7] S. Heidari, B. Rezaei, J. K. Sarma, and G. R. Boroun, Nucl. Phys. A **986**, 195 (2019); S. Heidari, B. Rezaei, and G. R. Boroun, Int. J. Mod. Phys. E **26**, 1750067 (2017); G. R. Boroun, B. Rezaei, and S. Heidari, Int. J. Mod. Phys. A **32**, 1750197 (2017).
[8] S. Atashbar Tehrani, Phys. Rev. C **86**, 064301 (2012); J. Sheibani, A. Mirjalili, and S. Atashbar Tehrani, *ibid.* **98**, 045211 (2018); H. Khanpour, M. Soleymaninia, S. A. Tehrani, H. Spiesberger, and V. Guzey, Phys. Rev. D **104**, 034010 (2021).
[9] N. Armesto, A. B. Kaidalov, C. A. Salgado, and K. Tywoniuk, Eur. Phys. J. C **68**, 447 (2010).
[10] F. Zaidi, H. Haider, M. S. Athar, S. K. Singh, and I. R. Simo, Phys. Rev. D **99**, 093011 (2019).
[11] J. L. Albacete, N. Armesto, A. Capella, A. B. Kaidalov, and C. A. Salgado, arXiv:hep-ph/0308050; N. Armesto *et al.*, Eur. Phys. J. C **29**, 531 (2003).
[12] S. J. Brodsky, V. E. Lyubovitskij, and I. Schmidt, Phys. Lett. B **824**, 136812 (2022).
[13] K. J. Eskola, P. Paakkinen, H. Paukkunen, and C. A. Salgado, Eur. Phys. J. C **77**, 163 (2017).
[14] R. D. Ball *et al.*, Eur. Phys. J. C **77**, 663 (2017).
[15] A. Accardi, T. J. Hobbs, X. Jing, and P. M. Nadolsky, Eur. Phys. J. C **81**, 603 (2021).
[16] A. Accardi *et al.*, Eur. Phys. J. A **52**, 268 (2016); D. P. Anderle *et al.*, Front. Phys. **16**, 64701 (2021).
[17] P. Agostini *et al.* (LHeC Collaboration and FCC-he Study Group), J. Phys. G **48**, 110501 (2021).
[18] H. Mäntysaari, PoS HardProbes**2018** (2018) 115.
[19] V. P. Goncalves, EPJ Web Conf. **112**, 02006 (2016).
[20] E. C. Aschenauer, S. Fazio, M. A. C. Lamont, H. Paukkunen, and P. Zurita, Phys. Rev. D **96**, 114005 (2017).

[21] J. Jalilianmarian and Y. V. Kovchegov, Prog. Part. Nucl. Phys. **56**, 104 (2006).
[22] J. L. Albacete and C. Marquet, Prog. Part. Nucl. Phys. **76**, 1 (2014).
[23] F. Gelis, E. Iancu, J. Jalilian-Marian, and R. Venugopalan, Annu. Rev. Nucl. Part. Sci. **60**, 463 (2010); L. D. McLerran and R. Venugopalan, Phys. Rev. D **49**, 3352 (1994); E. Iancu, A. Leonidov, and L. D. McLerran, Nucl. Phys. A **692**, 583 (2001).
[24] N. Armesto, J. Phys. G: Nucl. Part. Phys. **32**, R367 (2006); E. Sichtermann, Nucl. Phys. A **956**, 233 (2016).
[25] E. Chudakov *et al.*, PoS DIS**2016** (2016) 143.
[26] M. Klasen, K. Kovarik, and J. Potthoff, Phys. Rev. D **95**, 094013 (2017).
[27] Y. Hatta, Nucl. Phys. A **1005**, 121859 (2021); O. Brüning, A. Seryi, and S. Verdu-Andres, Front. Phys. **10**, 886473 (2022).
[28] E. Long, Technical Note T19-002 (2019).
[29] A. Capella *et al.*, Eur. Phys. J. C **5**, 111 (1998).
[30] M. M. Block, L. Durand, and P. Ha, Phys. Rev. D **89**, 094027 (2014).
[31] G. Soyez, Phys. Lett. B **655**, 32 (2007).
[32] C. Marquet, M. R. Moldes, and P. Zurita, Phys. Lett. B **772**, 607 (2017).
[33] M. A. Betemps and M. V. T. Machado, Eur. Phys. J. C **65**, 427 (2010).
[34] A. M. Stasto, K. Golec-Biernat, and J. Kwiecinski, Phys. Rev. Lett. **86**, 596 (2001).
[35] N. Armesto, C. A. Salgado, and U. A. Wiedemann, Phys. Rev. Lett. **94**, 022002 (2005).
[36] N. Armesto, C. Merino, G. Parente, and E. Zas, Phys. Rev. D **77**, 013001 (2008).
[37] I. I. Balitsky, Nucl. Phys. B **463**, 99 (1996); Phys. Rev. Lett. **81**, 2024 (1998); Phys. Lett. B **518**, 235 (2001).
[38] Y. V. Kovchegov, Phys. Rev. D **60**, 034008 (1999); **61**, 074018 (2000).
[39] L. N. Lipatov, Sov. J. Nucl. Phys. **23**, 338 (1976); E. A. Kuraev, L. N. Lipatov, and V. S. Fadin, Sov. Phys. JETP **45**, 199 (1977); I. I. Balitsky and L. N. Lipatov, Sov. J. Nucl. Phys. **28**, 822 (1978).
[40] C. Adloff *et al.* (H1 Collaboration), Eur. Phys. J. C **21**, 33 (2001); J. Breitweg *et al.* (ZEUS Colaboration), *ibid.* **12**, 35 (2000); S. Chekanov *et al.*, *ibid.* **21**, 443 (2001).
[41] J. L. Albacete, N. Armesto, J. G. Milhano, C. A. Salgado, and U. A. Wiedemann, Eur. Phys. J. C **43**, 353 (2005); Phys. Rev. D **71**, 014003 (2005).
[42] M. Krelina and J. Nemchik, Eur. Phys. J. Plus **135**, 444 (2020).
[43] L. Agozzino, P. Castorina, and P. Colangelo, Eur. Phys. J. C **74**, 2828 (2014).
[44] M. R. Adams *et al.* (E665 Collaboration), Phys. Rev. Lett. **68**, 3266 (1992); Z. Phys. C **67**, 403 (1995); M. Arneodo *et al.* (EMC Collaboration), Nucl. Phys. B **333**, 1 (1990); M. Arneodo *et al.* (NMC Collaboration), *ibid.* **441**, 12 (1995); P. Amaudruz *et al.* (NMC Collaboration), *ibid.* **441**, 3 (1995).
[45] B. Z. Kopeliovich, J. Nemchik, I. K. Potashnikova, and I. Schmidt, J. Phys. G: Nucl. Part. Phys. **35**, 115010 (2008); B. Z. Kopeliovich, J. Nemchik, N. N. Nikolaev, and B. G. Zakharov, Phys. Lett. B **324**, 469 (1994).
[46] K. J. Golec-Biernat and M. Wusthoff, Phys. Rev. D **59**, 014017 (1998).
[47] H. Kowalski, L. Motyka, and G. Watt, Phys. Rev. D **74**, 074016 (2006).
[48] B. Z. Kopeliovich, A. Schafer, and A. V. Tarasov, Phys. Rev. D **62**, 054022 (2000).
[49] J. Bartels, K. J. Golec-Biernat, and H. Kowalski, Phys. Rev. D **66**, 014001 (2002).
[50] A. H. Rezaeian, M. Siddikov, M. Van de Klundert, and R. Venugopalan, Phys. Rev. D **87**, 034002 (2013).